Radiation Properties of the Planar UWB Dipole Antenna in the Proximity of Dispersive Body Models

Tommi Tuovinen, Markus Berg, Kamya Yekeh Yazdandoost, Erkki Salonen, Jari Iinatti
Centre for Wireless Communications
P.O. Box 4500
90014 University of Oulu, Finland
+(358) 8 553 2894
E-mail: {givenname.surname}@ee.oulu.fi

ABSTRACT
In this paper, the radiation properties of a planar Ultra Wideband (UWB) dipole antenna are investigated both in the proximity of two different dispersive body tissue models and in free space. Simulation software utilizing Finite Integration Technique (FIT) is used for the examinations such that the antenna is operated through the range of 0 – 140 mm above the surface of the body models. Investigations are carried out in terms of (1) the realized maximum gain and total antenna efficiency behavior, (2) the 3D radiation patterns at specific distances, and (3) the reflections and absorption of the E-field distributions in the different positions. Simulation results are compared with the theoretical foundations. These studies are aim to exemplify the antenna – human body interactions in UWB Wireless Body Area Network (WBAN) applications.

Categories and Subject Descriptors
H.4.3 [**Information Systems Applications**]: Communications Applications – *computer conferencing, teleconferencing, and videoconferencing.*

General Terms
Performance, Theory.

Keywords
UWB WBAN systems, UWB dipole antenna, human body effect, reflections

1. INTRODUCTION
The systems kind of Ultra Wideband (UWB) Wireless Body Area Network (WBAN) communication has received lots of attention recent years. Development work in the fields of biomedical engineering and wearable hardware have generated possibilities, for instance, to the continuous monitoring of the patient's healthcare, which is one purpose of the use for WBANs [1]. In communications of this kind, data is collected from the patient and sent as electromagnetic (EM) waves by exploiting the antennas. Many investigations have proved that the human body has a strong effect on the antenna operation and performance, since the body in the proximity of the antenna loads it significantly [2], [3]. Especially, the body tissues in the area of the antenna's near-field regions are harmful. The propagation medium in WBANs is challenging since it comprises free space and lossy medium (referring to the body tissues). Hence the free space-body medium interface causes the reflections for the propagating EM waves.

This paper considers the link between WBAN on-body and off-body communications in UWB WBAN systems. The operation of the antenna that could be used as the main node meaning it is in connection with the node outside the body is investigated. The planar UWB dipole antenna is exploited in the examinations to cover the Federal Communications Commissions' (FCCs') UWB frequency band of 3.1 – 10.6 GHz. The realized gain and total antenna efficiency properties are investigated through the range of 0 – 140 mm away from the body. Then, the considerations of the 3D radiation patterns and E-field distributions are carried out for some specific distances, based on the observations with the gain and efficiency results. The results observed in simulations are compared with the theoretical foundations. All examinations are carried out as simulations with Computer Simulation Technology (CST) software [4].

2. UWB ANTENNA AND BODY MODELS
Fig. 1 presents the CST simulation model (dimensions in mm) of the planar UWB dipole, which is published first in [5] and includes both more results and analysis of the antenna's operation. The presented antenna was planned to be used on a side of 1.6 mm thick well-known FR4 substrate having ε_r = 4.3 and loss tangent of $tan\delta$ = 0.025 from CST material library. For the

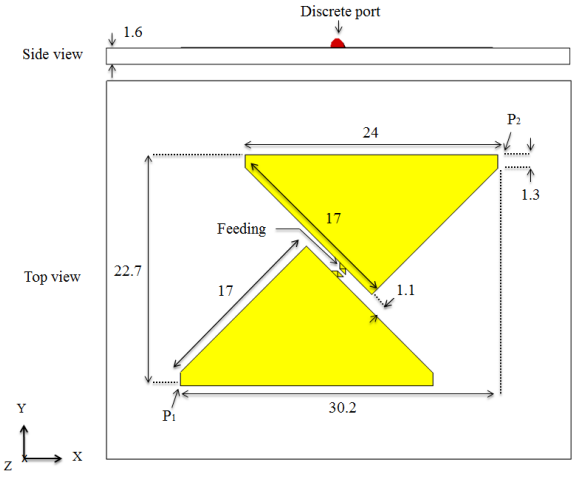

Figure 1. Simulation model of the UWB dipole antenna.

Permission to make digital or hard copies of all or part of this work for personal or classroom use is granted without fee provided that copies are not made or distributed for profit or commercial advantage and that copies bear this notice and the full citation on the first page. To copy otherwise, or republish, to post on servers or to redistribute to lists, requires prior specific permission and/or a fee.
Bodynets 2012, September 24-26, Oslo, Norway
Copyright 2012 ACM 1-58113-000-0/00/0010…$10.00.

Copyright © 2012 ICST
DOI 10.4108/icst.bodynets.2012.250133

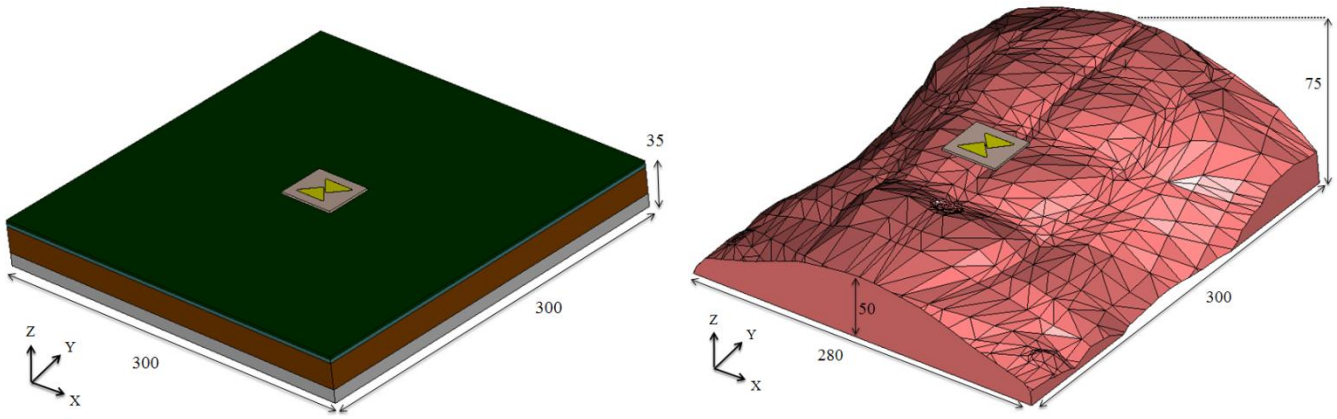

a) b)

Figure 2. Two dispersive body models to model the stomach: a) Layered human body model including (from the uppermost layer) skin, fat, muscle and bone tissues, and b) a piece of the whole human body model from the stomach area. The antenna and tissues are having the same coordinates, which are presented in the picture.

simulation purposes, the discrete port has been used. The largest dimension of the presented antenna (between points P_1 and P_2 in Fig. 1) is 37.3 mm. In this study, the UWB antenna was first simulated in free space and then in the proximity of both the layered body tissue model (Fig. 2a) and with a piece of the whole human body model (Fig. 2b). Body models were used to model a stomach area of human body. The material properties of the dispersive body models were adjusted based on the Debye Equation as follows.

Relative permittivity ε_r and permeability μ_r are close to 1 in the air hence the wave attenuates only in the agreement with the free space loss. Human body is a lossy material from the antenna point of view having complex permittivity ε (consisting of real ε' and imaginary ε'' parts) [6]. Body has the electrical losses as it is the material having conductivity σ unequal to zero. The losses are generated based on the Ohm's law (J = σE), as the electric field generates currents and the electric power will be worn as a heating [6]. Also, the damping of the vibrating dipole moments causes heat. The electrical dispersion can be defined based on the general Debye Equation as [7]-[9]

$$\varepsilon = \varepsilon' - j\varepsilon'' = \varepsilon_\infty + \frac{(\varepsilon_s - \varepsilon_\infty)}{1+j\omega\tau}, \quad (1)$$

where ε_s is static, i.e., low frequency permittivity and ε_∞ is infinite, i.e., high frequency permittivity, and the relaxation time τ is related to a relaxation frequency $f_r = 1/2\pi\tau$ [7]. In this study, the general Debye Equation is extended to be used with two relaxation constants, such that the static (zero frequency) dielectric can be given as [7], [8]

$$\varepsilon_s = \varepsilon_{s1} + \varepsilon_{s2} - \varepsilon_\infty, \quad (2)$$

and the Debye Equation becomes (called as the Debye 2nd order model) as [7], [8], [9]

$$\varepsilon = \varepsilon_\infty + \frac{\varepsilon_{s1} - \varepsilon_\infty}{1+j\omega\tau_1} + \frac{\varepsilon_{s2} - \varepsilon_\infty}{1+j\omega\tau_2}. \quad (3)$$

For the simulation results achieved here, ε_s and ε_∞ are approximated and defined based on the literature [7]-[9] and the online database [10]. Relaxation constants are adjusted according to [7] and [9]. The values used in the investigations are presented in Table 1. For a comparison, (real part of) ε_r values are also presented for the same tissues at 3 GHz and 10 GHz in Table 1 [10]. The size of layered model in this study is 300 (x) · 300 (y) · 35 (z) mm. A piece of the whole human body model with the size of 280 (x) · 300 (y) · 50 – 75 (z) mm is made of the dispersive (skin) material based on the Debye 2nd order model, too.

Table 1. Properties of tissues for simulations

	Tissues			
Tissue properties	**Skin**	**Fat**	**Muscle**	**Bone**
Epsilon static value 1, ε_{s1}	3399	35	3948	312.8
Epsilon static value 2, ε_{s2}	55.59	5.5	59.09	7.11
Epsilon infinity value, ε_∞	23	2.9	40	3.4
Relaxation time 1, τ_1 [ns]	46.2			
Relaxation time 2, τ_2 [ns]	0.091			
Density, ρ [kg/m^3]	1100	916	1041	1990
Thickness, t [mm]	2	3	20	10
Permittivity (ε_r) at 3 GHz	37.45	5.22	52.06	11.07
Permittivity (ε_r) at 10 GHz	31.29	4.60	42.76	8.12

3. Simulation Results

In this section, the first study demonstrates the effect of increasing the antenna-body model distance on the realized maximum gain and total antenna efficiency results (in Section 3.1). In Section 3.2, the 3D radiation patterns are presented in free space and in the proximity of the whole body model, and finally, the reflections and absorption due to the human body are demonstrated by the dint of E-field distributions in Section 3.3.

3.1 Antenna Gain and Efficiency in the Close Range of Body Models

The realized gain of the antenna can be defined as [11]

$$G(\theta, \phi) = e_0 D(\theta, \phi). \quad (4)$$

where θ and ϕ are the elevation and azimuth angles, D is the directivity and e_0 is the total antenna efficiency including reflection (mismatch) e_r, conduction e_c and dielectric e_d efficiencies as

$$e_0 = e_r e_c e_d = e_r e_{cd} = e_{cd}(1 - |\Gamma|^2), \quad (5)$$

where e_{cd} is the antenna radiation efficiency, and Γ is the voltage reflection coefficient of the input terminals of the antenna. The realized maximum gain and total antenna efficiency (in Fig. 3) were simulated at the different distances d between the antenna and human body models through the range of 0 – 140 mm (0 – 40

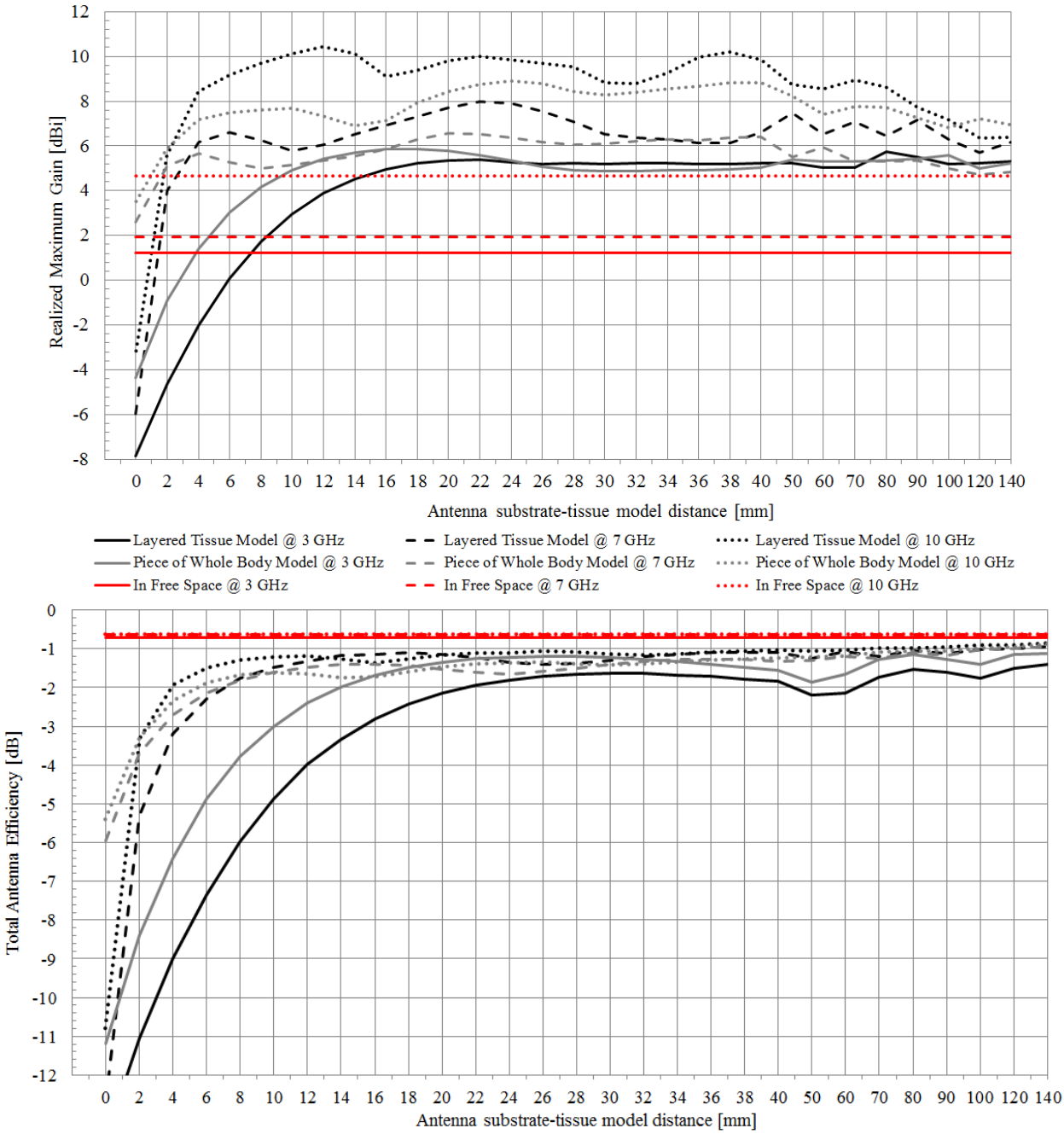

Figure 3. Simulated realized maximum gain (upper) and total antenna efficiency (lower) close the layered model and a piece of the whole body model through 0 – 140 mm (0 – 40 mm; steps of 2 mm, 40 – 100 mm; steps of 10 mm, 100 – 140 mm; steps of 20 mm).

mm; steps of 2 mm, 40 – 100 mm; steps of 10 mm, 100 – 140 mm; steps of 20 mm). In the near proximity of the layered and whole body models, the antenna was observed to be rather directive. Now, if we consider d = 20 mm, which could be a practical operational distance for the antenna located to the top of device, then the maximum gain is 4.0 dBi (3 GHz), 5.7 dBi (7 GHz) and 5.1 dBi (10 GHz) higher than in free space [in the proximity of the layered model] and 4.5 dBi (3 GHz), 4.6 dBi (7 GHz) and 3.7 dBi (10 GHz) [with the whole body model], respectively. The observed maximum gain results were even higher than in free space yet at d = 140 mm. Further, the higher maximum gain than in free space was already observed in the closeness of the layered model at d = 8 mm (3 GHz), d = 2 mm (7 GHz) and d = 2 mm (10 GHz), and at d = 6 mm (3 GHz), d = 2 mm (7 GHz) and d = 2 mm (10 GHz) with the whole body model.

By considering the total antenna efficiency results at d = 20 mm, 1.5 dB (3 GHz), 0.5 dB (7 GHz), and 0.5 dB (10 GHz) worse performance than in free space was observed in the proximity of the layered model, and 0.6 dB (3 GHz), 0.9 dB (7 GHz), and 0.8 dB (10 GHz) in the proximity of the whole body model, respectively. When comparing the performance on contact with the body models to the free space values, the drop of 13.7 dB (3 GHz), 12.7 dB (7 GHz), and 11.8 dB (10 GHz) was observed with the layered model, and the drop of 11.2 dB (3 GHz), 6.0 dB (7 GHz), and 5.4 dB (10 GHz) with the whole body model.

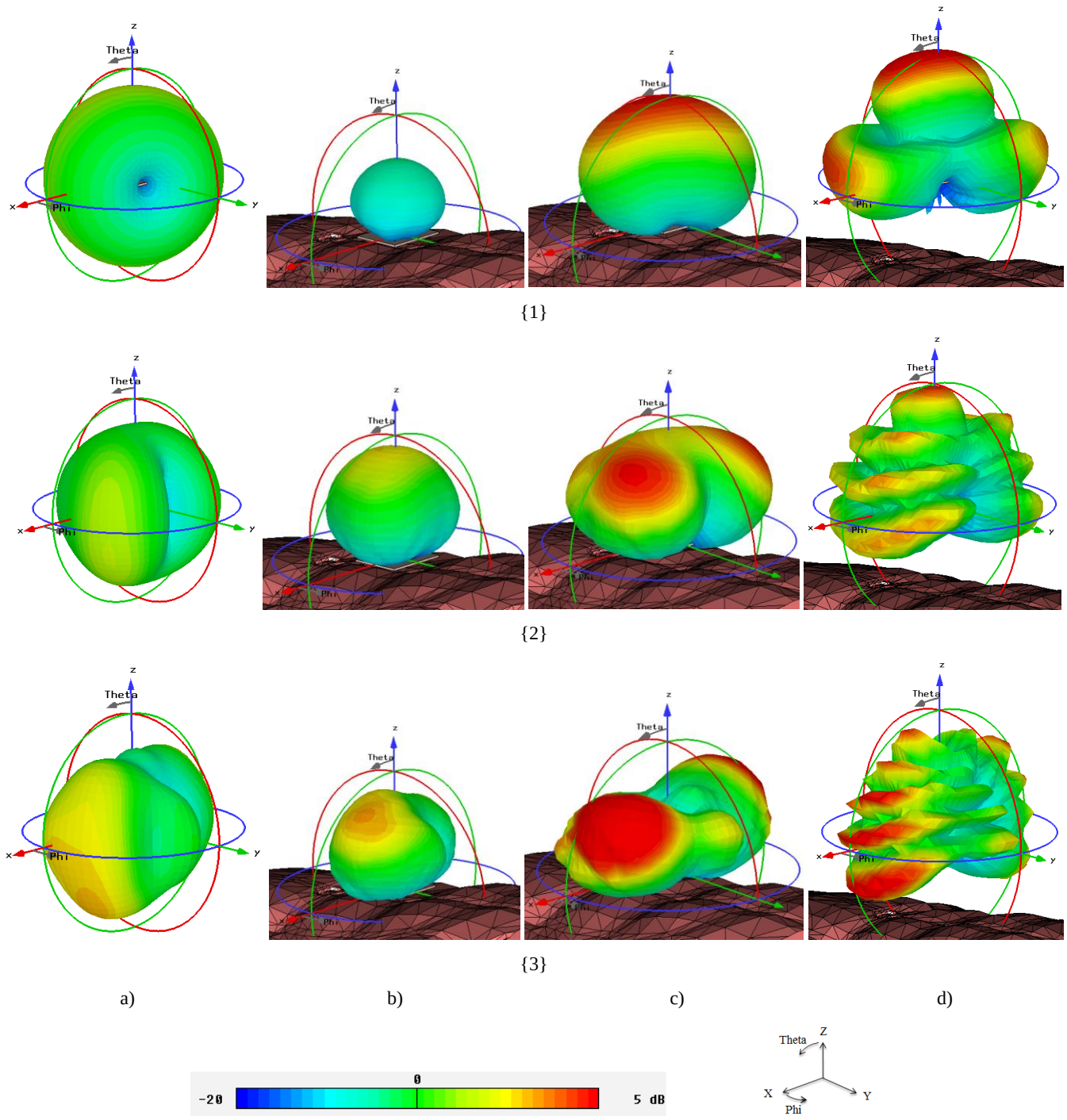

Figure 4. Simulated 3D radiation patterns (plots of realized gain) at frequencies of {1} 3 GHz, {2} 7 GHz, and {3} 10 GHz a) in free space, b) *d* = 0 mm, c) *d* = 10 mm, and d) *d* = 70 mm to a piece of the whole body model. Used co-ordinates are defined below the figure, of which origin is positioned to the place of feeding in each plots.

3.2 Radiation Patterns

Fig. 4 demonstrates the variation of the 3D radiation patterns (plots of realized gain) at the different positions at the frequencies 3 GHz, 7 GHz, and 10 GHz: *d* = 0, 10, and 70 mm to a piece of the whole body model (in Figs. 4b-d). The free space radiation patterns (in Fig. 4a) are presented as a reference, where rather omnidirectional radiation was observed over the entire UWB band. Once the antenna is operated on contact with the whole body model (in Fig. 4b), the concentration of the radiation was observed mostly in the z direction in comparison with the free space, as expected, due to the lossy body tissues right below the antenna. By increasing the operational distance *d* to 10 mm (in Fig. 4c), the expansion of the beam in the z direction can be seen, i.e., the red area in the patterns start to extend. We also analyzed patterns at *d* = 40, 70, 100, 140 mm, and the patterns were observed start to radiate slowly to the – z direction in higher distances. The shape of the patterns in higher distances were

noticed to contain many small maxima, as the reflected components affects to its shape, e.g., at d = 70. The reflection phenomenon is presented in pursuance of E-field distributions in Section 3.3 more clearly. However, in conclusion here, until d = 70 mm (in Fig. 4d) was achieved, the patterns were observed to radiate the largest proportion of the power to the space overhead xy-plane, i.e., hemisphere in the z direction. After d = 70mm, the patterns start to form slowly the similar shape than in free space, however, the patterns have uneven surface because of the reflection effect. The effect of the reflected components from the body as the maxima in the patterns can be observed at wavelength λ intervals, as $\lambda \approx 10$ cm at 3 GHz, and $\lambda \approx 3$ cm at 10 GHz, e.g., see d = 70 mm in Fig. 4d.

3.3 Reflections and absorption due to the human body

Here, in the link between WBAN off-body and on-body communications, generally, one of the exploited antennas is positioned close to the human body and may receive one field component from free space and many reflected components from the body at the link level.

In this study, the arrival of a plane wave to the flat interface between two media [(1) free space, and (2) human body] is theoretically considered. It is noted that a plane wave assumption is not valid however it is used to consider whether it is possible to interpret the simulation results with a plane wave assumption and a two-way propagation model (including direct and reflected components). Both the parallel and perpendicular polarizations are considered such that the wave is originated from the presented UWB dipole antenna (that is located at some distance away from the human body) towards the body. Here, the medium interface is set at xy-plane such that the wave travels in the direction of z-axis.

Generally, for the wave reflected in the direction of the surface normal, the reflection coefficient ρ can be written as [12]

$$\rho = \frac{\eta_2 - \eta_1}{\eta_2 + \eta_1}, \quad (6)$$

where $\eta_i = \sqrt{\mu/\varepsilon}$ is the wave impedance. Here, to calculate the components reflected from the different angles, the reflection coefficient ρ_{par} for the parallel wave (E-field vector is at the xz-plane) can be given as [12]

$$\rho_{par} = \frac{\sqrt{\frac{\varepsilon_{r2}}{\varepsilon_{r1}} - \sin\theta_i^2} - \frac{\varepsilon_{r2}}{\varepsilon_{r1}}\cos\theta_i}{\sqrt{\frac{\varepsilon_{r2}}{\varepsilon_{r1}} - \sin\theta_i^2} + \frac{\varepsilon_{r2}}{\varepsilon_{r1}}\cos\theta_i}, \quad (7)$$

where θ_i is the angle of incident wave relative to the normal of the interface, and the amount of reflected power can be presented as $|\rho_{par}|^2$. Correspondingly, for the perpendicular polarization (E-field vector is parallel to the y-axis), the reflection coefficient ρ_{per} can be presented as [12]

$$\rho_{per} = \frac{\cos\theta_i - \sqrt{\frac{\varepsilon_{r2}}{\varepsilon_{r1}} - \sin\theta_i^2}}{\sqrt{\frac{\varepsilon_{r2}}{\varepsilon_{r1}} - \sin\theta_i^2} + \cos\theta_i}. \quad (8)$$

By substituting numerical values [ε_{r1} = 1 (air), ε_{r2} = 35 (human body), and $0^o < \theta_i < 90^o$] to (7) is observed that the components, which across the free space-human body interface perpendicularly ($\theta_i = 0^o$), roughly 50% of the power reflect back in theory. From $\theta_i = 0^o$ to larger angles, the amount of reflected power start to decrease and the Brewster's angle is found at $\theta_i \approx 80^o$ where the reflection coefficient is close to zero. After's Brewster's angle at $85^o < \theta_i < 90^o$, the amount of reflected is power is very high, i.e., 100% at $\theta_i = 90^o$. Then, by using the same numerical values to (8) is observed that the amount of reflected power is also roughly 50% when $\theta_i = 0^o$, naturally. But in the perpendicular case when θ_i is increased from $\theta_i = 0^o$, the amount of reflected power is now started to increase by achieving 100% at $\theta_i = 90^o$.

Fig. 5 demonstrates the E-field distributions of the antenna at the different use cases: in free space, on contact with the whole body model, and with the distance of d = 10, 40, and 70 mm to the whole body model. The E-fields were not examined only in the presented use cases, but also with the multiple distances both with the layered and the whole body model. According to FCC, the limit of the power density spectrum in the UWB systems is – 41.3 dBm/MHz. Therefore, the maximum Effective Isotropic Radiated Power (EIRP) can be approximately 0.5 mW (–41.3 dBm/Mhz = 74 pW/Mhz => 0.556 mW) over the entire (3.1 – 10.6 GHz) UWB band. Here, the considerations are carried out, such that the E-fields are scaled to the EIRP = 0.5 mW

In free space (Fig. 5-{1}), the E-field radiates up and down away from the antenna in the frequencies of 3 GHz and 7 GHz. At 10 GHz, the highest amount of the radiation is observed along the surface of the antenna substrate however, naturally, there exist radiation also up and down away from the antenna. When the antenna was operated on contact with the layered body model, the strong absorption of the E-field was observed in comparison with the free space (in terms of magnitude), and the E-field radiate mostly away from the body. It should be noted here that in this situation (with the layered model), the E-field radiated symmetrically away from the antenna, as expected. On contact with the whole body model (Fig. 5-{2}), the E-field is not absorbed as significantly as with the layered model, because the whole body model does not load the antenna equally, i.e., the constant loading is prevented (corresponding behavior was reported in pursuance of the patterns). Further, the E-field distributions inside the tissue models (right below the antenna) are different between the layered and whole body models, naturally. On contact with the layered model, the E-field penetrated to the larger area (however, even though, the magnitude of the field is very low) while on the contact with the whole body model, the E-field is more focused to the direction of the normal of the body surface. From the simulation results can be noticed that the wave attenuates, naturally, more significantly inside the tissues in higher frequencies than in lower frequencies (with each model) as in the theory.

When analyzing Figs. 5-{3}&{4} (d = 10 and 40 mm) the decompositions of the E-fields because of the reflections of the body model were observed. In the case of the layered model, the E-field distributions were again symmetric. At d = 10 mm to the whole body model, the E-fields were very directive at 3 GHz, but also at 7 GHz meaning the largest proportion of the radiation was directed away from the body model. At 10 GHz, the strongest radiation was observed to be parallel to the body model. At d = 40 mm just a little radiation was observed inside the body models only at 3 GHz, and after d = 70 mm in Fig. 5-{5}, no radiation was observed inside the body models at any frequency. However, here should be emphasized that as the EIRP of 0.5 mW will be used in practical UWB WBAN system application, in that case, any radiation that could be harmful for the human body tissues will not exist at any distances, because of the extremely low power level of the UWB band. By increasing the distance further over d = 100 mm, the E-fields started slowly to remain that

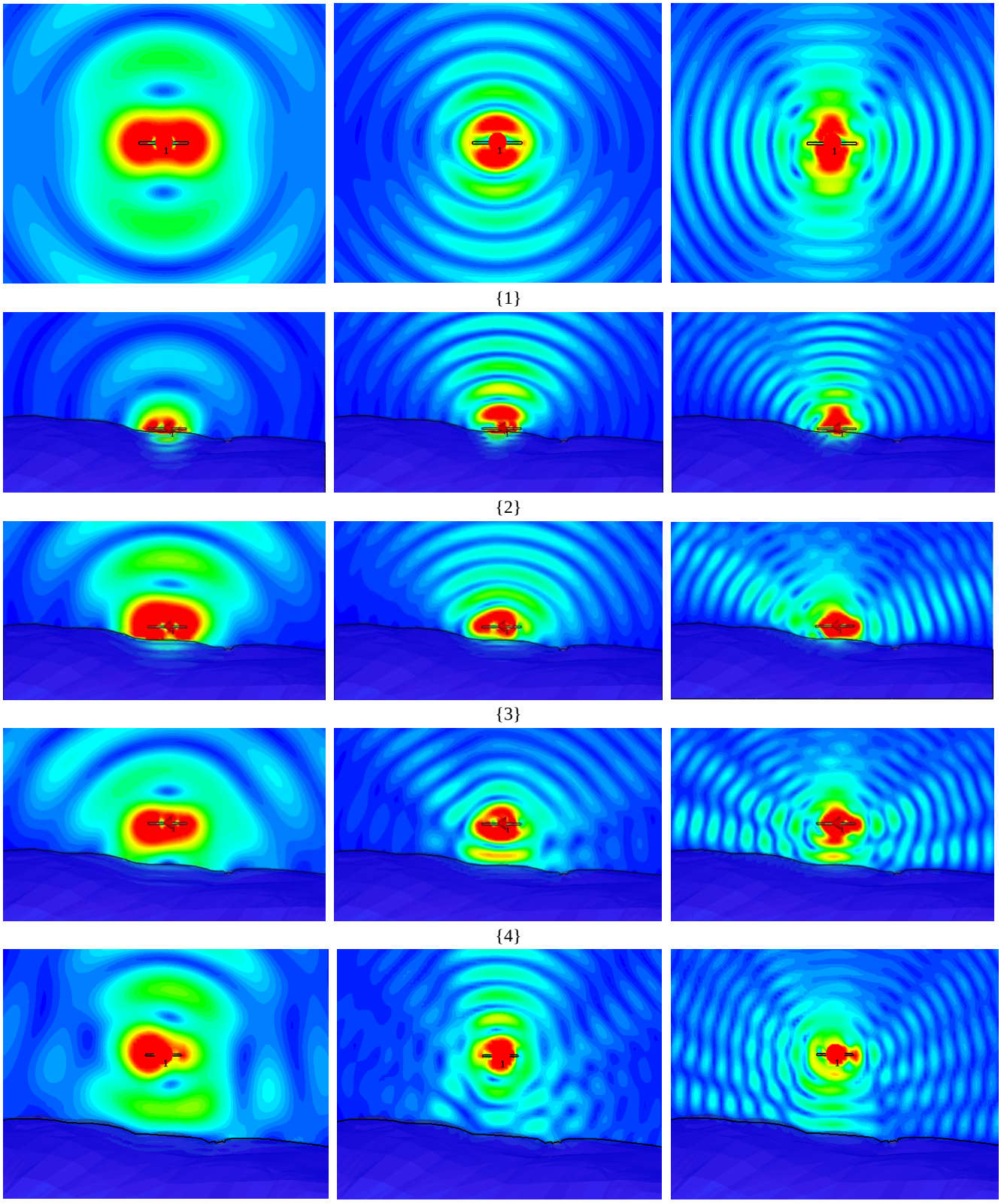

Figure 5. Simulated E-field distributions [V/m] at 0º phase at frequencies of a) 3 GHz), b) 7 GHz, and c) 10 GHz in the investigated use cases: {1} in free space, and {2} - {5} with the distances of *d* = 0, 10, 40 and 70 mm to the whole body model. The colour range is scaled through the range from 0 V/m (blue) to 0.1 V/m (red).

observed in free space. However, correspondingly with the patterns, there also exist reflected waves from the body interface.

Further, theoretical two-way propagation model for the parallel and perpendicular polarizations is formed by summing the direct ($\boldsymbol{E}_1$) and reflected ($\rho\boldsymbol{E}_1$) E-field components as

$$\boldsymbol{E}_{\text{tot}} = \boldsymbol{E}_1 + \rho\boldsymbol{E}_1 e^{-j2\pi d(1+\cos 2\,\theta)/\lambda \cos\theta}, \quad (9)$$

where d is the antenna-body distance. The power of $\boldsymbol{E}_{\text{tot}}$ is calculated with the different frequency and distance values as a function of angle θ (= θ_i = θ_r is the angle of reflection). The theoretical results with the two-way model were compared with the simulation results (both to the layered and whole body model). It was observed that in the close proximity of the body, i.e., 0 mm < d < 5 mm the two-way model does not show the reflected components correctly (those should appear mainly away from the body), which is due to the limitation of both the geometrical consideration and also the assumed point source (in reality the antenna radiates from the different points, but not as a point-form). However, at higher distances, the theoretical results were quite similar to the simulation results, even though many assumptions were done here. For example, if we set d = 70 mm and consider f = 3, 7, and 10 GHz with the two-way model, then the significant reflected components should appear at the angle θ_r = 0º and 70º at 3 GHz for the perpendicular polarization. Respectively, at θ_r = 0º, 40º, 60º and 80º for 7 GHz, and θ_r = 15º, 40º, 60º, 70º and 85º for 10 GHz. Comparing the values with Fig. 5-{5}, let's say, a rather good match is found. Correspondingly, a relatively good match is also found at d = 40 mm and at d = 10 mm, too. However, it should be noted that theoretical results consider only the flat, not the uneven, surface. Further, as stated earlier, the plane wave assumption is not valid here but we assume that the observed behavior can be explained such that when the antenna is farther away from the body, then the waves are more equivalent to the plane waves.

4. SUMMARY

This paper considers the radiation properties of the planar UWB dipole antenna. The examinations were started by evaluating the realized maximum gain and total antenna efficiency behavior at the range of 0 – 140 mm (0 – 40 mm; steps of 2 mm, 40 – 100 mm; steps of 10 mm, 100 – 140 mm; steps of 20 mm) away from the dispersive body tissue models. Secondly, the 3D radiation patterns were analyzed at the different distances (d = 0, 6, 10, 40, 70, 100, 140 mm) and finally, the E-field distributions were considered at the same distances. Two different dispersive body models, the layered body tissue model and a piece of the whole body model, were utilized in the investigations. When the antenna-body distance was analyzed, the maximum gain was observed to be even higher than in free space yet at the distance of 140 mm. In terms of the total antenna efficiency, roughly saying, 15 mm is the distance to achieve satisfactory performance. Based on the 3D patterns, the antenna was observed to be highly directive in the close proximity to the body such that antenna radiate mainly in the z direction, i.e., away from the body. By increasing the distance, the beam of pattern was started to slowly open and further start to radiate towards the body. The patterns were noticed be rough, i.e., uneven surface, because of the reflections from the body. Corresponding behavior was observed when analyzing the E-field distributions.

These investigations and considerations are based on the simulations and theoretical results. In time of writing this paper, the prototype of the antenna is already fabricated and verified the corresponding free space operation than in simulations. Measurements will be provided as a next step of this work.

5. ACKNOWLEDGMENTS

This work has funded by the Finnish Funding Agency for Technology and Innovation (TEKES) through Wireless Body Area Network for Health and Medical Care (WiBAN-HAM) project. Tauno Tönning, Emil Aaltonen and TES Foundations are also acknowledged.

6. REFERENCES

[1] Hall, P.S. and Hao, Y. 2006. *Antennas and Propagation for Body-Centric Wireless Communications*. Norwood, MA: Artech House Inc.

[2] Chen, Z.N., Cai, A., See, T.S.P., Qing, X. and Chia, M.Y.W. 2006. Small Planar UWB Antennas in Proximity of the Human Head. In *IEEE Trans. on Microwave Theory and Techniques*, Vol. 54, No. 4 (April 2006), 1846-1857. DOI = 10.1109/TMTT.2006.872059.

[3] See, T.S.P., Chen, Z.N. and Qing, X.M. Proximity Effect of UWB Antenna on Human Body. In *Proceedings of the APMC Microwave Conference* (Singapore, December 7-10, 2009). DOI = 10.1109/APMC.2009.5385342.

[4] Computer Simulation Technology (CST). [Online]. DOI = http://www.cst.com/.

[5] Tuovinen, T., Berg, M., Yekeh Yazdandoost, K., Salonen, E. and Iinatti, J. 2012. Human Body Effect on the Polarization Properties of the New UWB Dipole Antenna in WBAN UWB Applications. Submitted to *Bodynets 2012* (Oslo, Norway, September 24-26, 2012).

[6] Pozar, D. M. 1998. *Microwave Engineering*. England: John Wiley & Sons Ltd, 2nd ed.

[7] Barnes, F. S. and Greenebaum, B.. 2007. *Bioengineering and Biophysical Aspects of Electromagnetic Fields*. Taylor & Francis Group.

[8] Gandhi, O.P., Gao, B.Q. and Chen, J.Y. 1993. A Frequency-Dependent Finite-Difference Time-Domain Formulation for General Dispersive Media. In *IEEE Trans. on Ant. and Propag.*, Vol. 41, No. 4 (April 1993), 658-665. DOI = 10.1109/22.231661.

[9] Gandhi, O.P. and Furse, C.M. 1997. Currents Induced in the Human Body for Exposure to Ultrawideband Electromagnetic Pulse. In *IEEE Trans. on Electrom. Compat.*, Vol. 39, No. 2 (May 1997), 174-180. DOI = 10.1109/15.584941.

[10] Italian National Research Council. [Online]. Calculation of the Dielectric Properties of Body Tissues in the frequency range 10 Hz – 100 GHz. DOI = http://niremf.ifac.cnr.it/tissprop/htmlclie/htmlclie.htm.

[11] Balanis, C. A. 2005. *Antenna Theory Analysis and Design*. New Jersey: John Wiley & Sons Ltd, 3rd ed.

[12] Räisänen, A. V. and Lehto, A. 2003. *Radio Engineering for Wireless Communication and Sensor Applications*. Norwood, MA: Artech House Inc.